Regional characteristics of NO_2 column densities from Pandora observations during the MAPS-Seoul campaign

Heesung Chong[1], Hana Lee[1], Ja-Ho Koo[1], Jhoon Kim[1,2], Ukkyo Jeong[3], Woogyung Kim[3], Sang-Woo Kim[4], Jay R. Herman[3], Nader K. Abuhassan[3], Junyoung Ahn[5], Jeong-Hoo Park[5], Sang-Kyun Kim[5], Kyung-Jung Moon[5], Won-Jun Choi[5], and Sang Seo Park[4*]

[1]Department of Atmospheric Sciences, Yonsei University, Seoul, South Korea
[2]Harvard – Smithsonian Center for Astrophysics, Cambridge, Massachusetts, USA
[3]NASA Goddard Space Flight Center, Greenbelt, Maryland, USA
[4]School of Earth and Environmental Sciences, Seoul National University, Seoul, South Korea
[5]National Institute of Environmental Research, Incheon, South Korea

Abstract

Vertical column density (VCD) of nitrogen dioxide (NO_2) was measured using Pandora spectrometers at six sites on the Korean Peninsula during the Megacity Air Pollution Studies-Seoul (MAPS-Seoul) campaign from May to June 2015. To estimate the tropospheric NO_2 VCD, the stratospheric NO_2 VCD from the Ozone Monitoring Instrument (OMI) was subtracted from the total NO_2 VCD from Pandora. European Centre for Medium-Range Weather Forecasts (ECMWF) reanalysis wind data was used to analyze variations in tropospheric NO_2 VCD caused by wind patterns at each site. The Yonsei/SEO site was found to have the largest tropospheric NO_2 VCD (1.49 DU on average) from a statistical analysis of hourly tropospheric NO_2 VCD measurements. At rural sites, remarkably low NO_2 VCDs were observed. However, a wind field analysis showed that trans-boundary transport and emissions from domestic sources lead to an increase in tropospheric NO_2 VCD at NIER/BYI and KMA/AMY, respectively. At urban sites, high NO_2 VCD values were observed under conditions of low wind speed, which were influenced by local urban emissions. Tropospheric NO_2 VCD at HUFS/Yongin increases under conditions of significant transport from urban area of Seoul according to a correlation analysis that considers the transport time lag. Significant diurnal variations were found at urban sites during the MAPS-Seoul campaign, but not at rural sites, indicating that it is associated with diurnal patterns of NO_2 emissions from dense traffic.

Keywords: Pandora; NO_2; MAPS-Seoul

* Corresponding author. Tel: 82-2-880-5743; Fax: 82-2-887-0210
E-*mail address*: pss8902@gmail.com

INTRODUCTION

Nitrogen dioxide (NO_2) is an important chemical species in both tropospheric and stratospheric chemistry (e.g., Crutzen, 1979; Brasseur et al., 1998). NO_2 mainly affects air quality in the troposphere through its role in chemical processes with ozone (O_3) and other trace gases (e.g., Seinfeld, 1988; Solomon et al., 1999; IPCC, 2007; Choi et al., 2008, 2009). In addition, long-term exposure to high concentrations of NO_2 causes respiratory and cardiovascular diseases (e.g., Chitano et al., 1995; Bayram et al., 2001; von Klot et al., 2005). Emission sources of NO_2 differ between the troposphere and stratosphere (Lee et al., 1997; Barton and Atwater, 2002; Galloway et al., 2004). In the stratosphere, the main source of NO_2 is oxidation of nitrous oxide (N_2O) and other sources include lightning and biomass burning (e.g., Liley et al., 2000; Barthe et al., 2007; Allen et al., 2010; Bucsela et al., 2013). In the troposphere, anthropogenic activities, including fossil fuel combustion and vehicle emissions, are the dominant sources of NO_2, along with some contributions from soil emissions and lightning (Zhang et al., 2003; Hudman et al., 2007; Choi et al., 2008, 2009). Because of the diversity of nitrogen oxides chemical reactions and emission sources, spatial distributions of NO_2 typically show regional differences. For these reasons, accurate observations of the spatial distribution of NO_2 are important.

Several measurement platforms for tropospheric gases, including NO_2, have been developed in recent decades. In particular, tropospheric column NO_2 is widely monitored using ground- and satellite-based platforms that make use of the spectral absorption features of NO_2. For example,

57 the Brewer spectrophotometer can estimate total column NO_2 using direct solar radiation at
58 several specific wavelengths (e.g., Brewer et al., 1973; Kerr et al., 1988, 1989; Cede et al., 2006;
59 Diemoz et al., 2014). In addition, several instruments have been used to measure NO_2 column
60 densities using differential optical absorption spectroscopy (DOAS) methods (e.g., Boersma et al.,
61 2004; Castellanos et al., 2015; Chimot et al., 2016) applied to sunlight scattered along the zenith
62 (Van Roozendael et al., 1997; Liley et al., 2000) or scattered in multiple directions (e.g., Sinreich
63 et al., 2005; Irie et al., 2008; Lee et al., 2009a, b).

64 Recently, the Pandora spectrometer was developed by Goddard Space Flight Center (GSFC) at
65 the National Aeronautics and Space Administration (NASA) for the estimation of trace gases
66 using direct sunlight (Herman et al., 2009; Cede, 2011). The Pandora system is an array detector
67 spectrometer with a temperature control system. A solar tracking system is also included to allow
68 constant direct-sunlight observations. Using this optical system, the Pandora instrument can
69 continuously observe direct radiance with high temporal resolution. This instrument has been
70 used to obtain the total column amount of trace gases, including O_3 and NO_2 (Herman et al., 2009;
71 Tzortziou et al., 2012).

72 In South Korea, the first two Pandora instruments were installed in 2012 at Yonsei University
73 in Seoul and Pusan National University in Busan for trace gas observations during the Distributed
74 Regional Aerosol Gridded Observation Networks-North East Asia (DRAGON NE-Asia)

75 campaign. Since the initial installations, several instruments were installed additionally in
76 different regions in Korea. The main purpose of Pandora network in Korea was to conduct
77 observations for the Megacity Air Pollution Studies-Seoul (MAPS-Seoul; May to June, 2015) and
78 Korea-United States Air Quality Study (KORUS-AQ; May to June, 2016), field campaigns in
79 Korea aimed to monitor and understand air quality (https://espo.nasa.gov/korus-
80 aq/content/KORUS-AQ_Science_Overview_0). It also supports studies associated with the
81 planned satellite mission for the Geostationary Environmental Monitoring Spectrometer (GEMS;
82 Kim 2012), designed to study atmospheric chemical composition and reaction mechanisms over
83 East Asia (Kim et al., 2017). Measurements from Pandora instruments in South Korea have been
84 utilized for multi-year analyses and the validation of total O_3 measurements (Baek et al., 2017;
85 Kim et al., 2017). Although the data quality of total O_3 from the Pandora spectrometers differs by
86 instrument, the difference in total O_3 between Pandora and other instruments has been less than
87 2% in all comparison studies to date (Baek et al., 2017; Kim et al., 2017).
88 Because variations in total O_3 can primarily be attributed to changes in the stratosphere, the
89 pattern of total O_3 density shows a weak dependence on regional or local emissions near the
90 observation sites. In contrast, NO_2 column is affected primarily by vehicle emissions, industrial
91 activities, and local short-range transport in the troposphere. Although some previous work
92 analyzed the effect of the long-range transport of NO_2 (e.g., Donnelly et al., 2015), the lifetime of

93 NO_2 near the surface is on the order of hours to days (Seinfeld and Pandis, 2012), indicating that
94 a careful approach is required for analyses of the effects of regional-scale transport on variations
95 in NO_2 concentrations.

96 Thus, the objective of this study is to investigate the effects of local air-mass transport from
97 NO_2 sources on vertical column densities (VCD) of tropospheric NO_2 from Pandora observations.
98 As a preliminary study for the KORUS-AQ campaign, we analyzed the regional characteristics of
99 NO_2 measurements at six Pandora sites obtained during the MAPS-Seoul campaign while
100 considering wind patterns and the locations of regional emission sources. Using these findings,
101 we report the characteristics of NO_2 VCD during the MAPS-Seoul campaign from May 18 to
102 June 14, 2015 in South Korea.

103

104 **DATA AND ANALYSIS**

105

106 Variations in tropospheric NO_2 VCD were analyzed at six Pandora sites. Also, the
107 characteristics of NO_2 transport during the MAPS-Seoul campaign were investigated using the
108 wind information from European Centre for Medium-Range Weather Forecasts (ECMWF)
109 reanalysis data. To evaluate the characteristics of transport in the troposphere at the Pandora
110 observation sites, we obtained tropospheric NO_2 VCD by subtracting Ozone Monitoring
111 Instrument (OMI) stratospheric NO_2 VCD from Pandora total NO_2 VCD.

112

113 ***NO_2 from Pandora***

114 The Pandora spectrometer system is configured with mounting systems for sun-tracker and
115 sky-scanner controls, and a temperature stabilizing system for radiometric calibration (e.g.,
116 Herman et al., 2009; Tzortziou et al., 2012, 2013). The Pandora instruments in Korea are direct-
117 sun (DS) spectrometer systems with a spectral range of 280–525 nm (spectral resolution: 0.42–
118 0.52 nm), and are used to measure the absorption spectra of trace gases (Baek et al., 2017). The
119 first two Pandora spectrometers in Korea were installed at Yonsei University and Pusan National
120 University in March 2012 to measure total column NO_2 and O_3. These instruments participated in
121 the DRAGON-NE Asia campaign in South Korea at that time. Since the initial installations, six
122 Pandora observation sites came into operation over the Korean Peninsula as part of the MAPS-
123 Seoul campaign. Table 1 summarizes the locations and altitudes of the Pandora observation sites
124 operated during the campaign, and Figure 1 shows their locations with a ten-year (2005–2014)
125 mean tropospheric NO_2 VCD in Dobson Units (DU; 1 DU = 2.69×10^{16} molecules/cm^2) from
126 Level 3 OMI NO_2 product (OMNO2d) in May and June, and mean surface wind reanalysis data
127 from ECMWF for the same period.

128 Total NO_2 VCD was retrieved using the spectral fitting method described by Herman et al.
129 (2009). For the analysis, we used Pandora level-3 data, which includes the normalized root-mean
130 square error (normalized RMS), uncertainties in the NO_2 column, and the index of the filter

131 wheel position. Threshold values for quality control that we used were 0.05 DU for both
132 normalized RMS and uncertainties in the NO_2 column, respectively.

133 Pandora provides total NO_2 VCD every 80 seconds (e.g., Tzortziou et al., 2012; Yun et al.,
134 2013). We converted the Pandora total NO_2 VCDs to hourly values by averaging over a ±30-min
135 window every hour. In this procedure, the resultant hourly data which have less than three points
136 in their windows (~5% of total measurable points in an hour) were excluded. Total VCD includes
137 both stratospheric and tropospheric NO_2. However, tropospheric NO_2 VCD usually dominates
138 total NO_2 VCD variations near urban and industrial areas. To accurately estimate tropospheric
139 NO_2 VCD from Pandora observations, stratospheric NO_2 information is required. For this
140 information, we used the OMI standard product, which is explained in detail in the following sub-
141 section. Thus, tropospheric NO_2 VCD was estimated for the MAPS-Seoul campaign at each
142 observation site, and the number of data points at each site is listed in Table 2. Because of
143 problems with the tracker cable on the Pandora instrument at the Yonsei/SEO site beginning May
144 29, the number of valid data points at this site was less than half the number of data points at the
145 other five Pandora observation sites.

146 The six Pandora sites were selected to include both urban and rural areas on the Korean
147 Peninsula. Figure 2 shows the topography (in color) of the regions around the observation sites.
148 The Baengnyeongdo site operated by National Institute of Environmental Research (NIER)

149 (NIER/BYI; Figure 2a) and the Anmyeondo site operated by Korean Meteorological Agency
150 (KMA) (KMA/AMY; Figure 2d) are located in coastal areas far from industrial and urban regions.
151 The NIER/BYI site is on an island located in northwest South Korea and is the closest site to
152 China. KMA/AMY is also located in the western coastal region of Korea. The NIER/BYI and
153 KMA/AMY sites are relatively free from the urban pollution and therefore were used as
154 background sites in this study. The Busan (operated by Pusan National University) (PNU/Busan;
155 Figure 2f) site and the Gwangju (operated by Gwangju Institute of Science and Technology;
156 GIST) (GIST/Gwangju; Figure 2e) site are located on the northern part of the urban areas in
157 Busan and Gwangju, respectively. These two cities are respectively the 2nd and 6th most
158 populous cities in South Korea. The Seoul (operated by Yonsei University) (Yonsei/SEO; Figure
159 2b) site and the Yongin (operated by Hankuk University of Foreign Studies; HUFS)
160 (HUFS/Yongin; Figure 2c) site are located in the Seoul metropolitan area (SMA); however, these
161 two sites have different characteristics. The Yonsei/SEO site is at the center of the Seoul urban
162 area, while the HUFS/Yongin site is in a suburban area 40 km southeast and downwind of Seoul.
163 Therefore, the HUFS/Yongin site is expected to be affected by transport from the urban area of
164 Seoul.
165
166 ***Stratospheric NO_2 from OMI***

167 The OMI instrument was designed to observe total column amounts of several trace gases
168 including NO_2, and thus aid analyses of air quality and assessments of the climate effects of
169 changes in chemical composition. OMI was launched in 2004 onboard the Aura satellite and
170 measures backscattered solar light in the ultra violet (UV)-visible range (270–500 nm) using
171 three different channels (two UV and one visible; e.g., Levelt et al., 2006; Buchard et al., 2008).
172 The nominal spatial resolution is from 13 × 24 km^2 (at nadir) to 28 × 150 km^2 (at the edge of the
173 swath). Because the Aura is a sun-synchronous satellite with a 98° inclination angle, daily values
174 over the Korean Peninsula from OMI were obtained from data from one or two overpasses per
175 day in the afternoon. The nadir 13 × 24 km^2 pass was obtained close to 13:30 local time.
176 The NO_2 VCD from OMI is based on the level-2 standard product of NASA's version 3 OMI
177 NO_2 (OMNO2) dataset. For the retrieval of NO_2, spectral radiance data from 405 to 465 nm in
178 the visible spectrum were used to estimate slant column amounts (Bucsela et al., 2013). As part
179 of improvements to the retrieval algorithm between versions 2 and 3, chemical transport model
180 simulations with time-dependent emissions were adopted to account for variations in the vertical
181 profiles for air mass factor calculations (Ialongo et al., 2016; Krotkov et al., 2017). The OMNO2
182 provides total, tropospheric, and stratospheric NO_2 VCD. Thus, OMI stratospheric NO_2 data can
183 be used to estimate the tropospheric NO_2 VCD from Pandora observations. Stratospheric NO_2 is
184 affected by chemical reactions and lightning activity (Noxon, 1979; Zhang et al., 2000; Wenig et

al., 2004) and thus varies spatiotemporally. We sampled the stratospheric NO_2 VCD from OMI for each Pandora station, and thus the tropospheric NO_2 VCD from Pandora data was calculated as

$$VCD_{PAN,Trop} = VCD_{PAN,Tot} - VCD_{OMI,Strat}, \quad (1)$$

where $VCD_{PAN,Trop}$, $VCD_{PAN,Tot}$, and $VCD_{OMI,Strat}$ are the tropospheric and total NO_2 VCD from Pandora, and the stratospheric NO_2 VCD from OMI, respectively.

For spatial co-location with Pandora, we selected the OMI pixels within 20 km from each Pandora site. While the Pandora total NO_2 VCD was calculated for each hour, OMI values occur only once daily, in the afternoon. This is one potential error source for using OMI to estimate tropospheric NO_2 VCD from the Pandora observations. In this study, we assumed the temporal and spatial distribution of stratospheric NO_2 was stable throughout the day and over the 20 km window. This approach is adapted from previous studies (e.g. Knepp et al., 2013; Kollonige et al., 2017) which estimated tropospheric NO_2 VCD by subtracting OMI stratospheric NO_2 VCD from Pandora total column NO_2 observations, assuming constant stratospheric NO_2 column on a daily basis under polluted conditions. In less polluted regions, such as NIER/BYI in this study, negative tropospheric NO_2 values can occur occasionally with this method. In addition, during

203 the stratosphere-troposphere separation procedure for OMI NO_2 standard product, the
204 stratospheric NO_2 VCD is smoothed interpreting smaller-scale features than approximately 300
205 km in the initial estimate as tropospheric (Bucsela et al., 2013). Thus, assuming negligible spatial
206 variability in the 20 km window, which is much smaller, is reasonable. Figure 3 shows the total
207 NO_2 VCD observed from Pandora and sampled stratospheric NO_2 VCD from OMI for each site
208 during the MAPS-Seoul campaign. Tropospheric NO_2 dominates total NO_2 VCD in the SMA (at
209 Yonsei/SEO and HUFS/Yongin), and PNU/Busan, as can be inferred from Figure 1. Despite
210 showing lower levels of total NO_2 compared to those sites, the amounts and variability of NO_2 in
211 the stratosphere at NIER/BYI, KMA/AMY, and GIST/Gwangju are relatively small in
212 comparison to total, allowing stratospheric NO_2 VCD to be assumed constant on a daily basis.
213 However, there were days for which no data from OMI were available within 20 km from a
214 ground-based observation site. In this case, the averaged OMI stratospheric NO_2 VCD for that
215 particular site over the course of the campaign period was used (red dots in Figure 3b).
216
217 ***Wind data***
218 To analyze the transport characteristics of NO_2 at the observation sites, we used the wind speed
219 and wind direction at the surface. Because surface wind varies significantly with surface
220 conditions over small spatial scales, high-resolution wind information is required. For the wind
221 analysis, U and V (west–east and south–north, respectively) wind components at 10 m altitude

222 from ECMWF reanalysis interim data (hereafter ERA-Interim) were used in this study (Dee et al.,
223 2011; http://apps.ecmwf.int/datasets/). To decrease local surface-condition effects on wind, the
224 ECMWF ERA-Interim were used at the highest available horizontal resolution, 0.125° × 0.125°.
225 The U and V wind components from ERA-Interim were interpolated to the latitude and
226 longitude of the respective Pandora sites. Then we converted them to the wind speed and
227 direction at each site. The original reanalysis data have a temporal resolution of 6 hours. Thus,
228 wind information was interpolated to a 1-hour resolution from the original 6-hour resolution after
229 the spatial interpolation, for temporal co-location with the NO_2 data.
230

231 **RESULTS AND DISCUSSION**
232

233 Figure 4 shows a time series of hourly-based tropospheric NO_2 VCD from the Pandora
234 observations. During the MAPS-Seoul campaign period, tropospheric NO_2 VCDs at NIER/BYI
235 and KMA/AMY were remarkably low, ranging from -0.07 to 0.45 DU and from 0.03 to 0.95 DU,
236 respectively. However, large NO_2 VCDs were observed, up to 4.70 DU at Yonsei/SEO and 2.04
237 DU at PNU/Busan. While the difference between the maximum and minimum during the whole
238 campaign period was less than 1 DU at NIER/BYI and KMA/AMY, a variation of 3.96 DU was
239 observed in a single day on May 28 at Yonsei/SEO. Tropospheric NO_2 VCD was always below
240 0.45 DU at the NIER/BYI site because of the large distance from emission sources. At the

241 NIER/BYI site, the tropospheric NO_2 VCD temporarily increased on May 19 and 21, but
242 otherwise remained small and constant. Negative values were found at this site, which were
243 generated by subtraction of OMI stratospheric NO_2 VCD larger than Pandora total NO_2 VCD.
244 However, the number of them was less than 2% of the total data points. In a diurnal scale,
245 variations in tropospheric NO_2 were clearly observed at the Yonsei/SEO, HUFS/Yongin, and
246 PNU/Busan sites, which are the sites nearest to large urban areas. However, the diurnal cycle in
247 tropospheric NO_2 VCD at GIST/Gwangju was not as strong. It was similar to what was observed
248 at KMA/AMY and NIER/BYI, although the GIST/Gwangju site is located near an urban area
249 (see also Figure 9).

250 Table 2 and Figure 5 present details of the hourly tropospheric NO_2 VCDs during the
251 MAPS-Seoul Campaign. The Yonsei/SEO site showed the maximum mean tropospheric NO_2
252 VCD (1.49 ± 0.68 DU) among the six sites during the campaign period. Even the minimum
253 tropospheric NO_2 VCD at this site was 0.60 DU, which is larger than the maximum value of
254 tropospheric NO_2 VCD at the NIER/BYI site (0.45 DU), representing the huge NO_2 emissions in
255 Seoul. In addition, the HUFS/Yongin and PNU/Busan sites had similar tropospheric NO_2 VCD
256 levels. The HUFS/Yongin site had the third largest average tropospheric NO_2 VCD (0.67 ± 0.49
257 DU), following PNU/Busan (0.72 ± 0.39 DU), indicating that huge local emissions in Seoul also
258 lead to high NO_2 concentrations around the SMA. The NO_2 VCD in the troposphere at

GIST/Gwangju (0.26 ± 0.14 DU) was comparable to that in KMA/AMY (0.18 ± 0.14 DU). Although the GIST/Gwangju site is located in an urban area, levels of tropospheric NO_2 VCD resembled those at the suburban and rural sites, because the industrial region around Gwangju is small. As can be seen from the box-and-whisker plots in Figure 5, all the sites are skewed in the positive direction. From the results so far, the statistics of tropospheric NO_2 were identified for each of the Pandora sites during the MAPS-Seoul campaign. However, even if the distribution of tropospheric NO_2 VCDs is similar between sites, major contributors to the amounts may differ by local emissions and transport patterns.

For better understanding of major contributors to tropospheric NO_2 VCD at each site, we need to examine the NO_2 VCD change in accordance with the wind pattern. Figure 6 shows polar plots of tropospheric NO_2 VCD, along with wind speed and direction at the six Pandora sites. Because of the regional characteristics of wind and the short campaign period, it is likely that not all wind patterns in South Korea are included in the analysis (e.g., seasonal wind pattern). However, this analysis indicates how wind pattern affects the regional characteristics of tropospheric NO_2 during the MAPS-Seoul campaign. In most cases, the wind speed did not exceed 10 m/s at the observation sites, and westerly wind was dominant over easterly wind. This is consistent with the general wind pattern over the Korean peninsula in May and June (see Figure 1). Despite the limited number of observed wind patterns, Figure 6 clearly shows a change in tropospheric NO_2

277 VCD as the wind field changes. At all the Pandora observation sites, remarkably high
278 tropospheric NO_2 VCDs at each site were found for specific wind fields. However, these wind
279 field characteristics differ among the observation sites.

280 At two urban sites, Yonsei/SEO (Figure 6b) and PNU/Busan (Figure 6f), high tropospheric
281 NO_2 VCD values were found under conditions of southerly wind with low wind speed (<4 m/s).
282 The GIST/Gwangju (Figure 6e) site also showed high VCD values under these wind conditions,
283 but the change in NO_2 VCD was smaller and may not be significant. This finding indicates that
284 local NO_2 emissions have huge contribution to the enhancement of tropospheric NO_2 at
285 Yonsei/SEO and PNU/Busan during the campaign period.

286 Specific wind fields at the NIER/BYI (Figure 6a) and KMA/AMY (Figure 6d) sites were also
287 associated with high NO_2 VCD: westerly wind with speeds of 4–6 m/s for NIER/BYI, and
288 easterly wind with speeds of 2–4 m/s for KMA/AMY. These two observation sites are in rural
289 areas with weak local emissions. Therefore, high VCD values can be attributed to transport.
290 However, the NO_2 transport patterns differ between the two sites. As seen in Figure 2, NIER/BYI
291 borders the Yellow sea on the west, while the regions to the east of the KMA/AMY site are land
292 surfaces. Therefore, high concentrations of NO_2 at the NIER/BYI site are thought to be due to
293 trans-boundary transport (e.g., Lee et al., 2014), while those at the KMA/AMY site are attributed
294 to the transport of domestic (Korean) emissions near the observation sites. Large domestic

295 sources of NO_2 around the KMA/AMY site include power plants and industrial activity. The
296 KMA/AMY site is close to many power plants that provide power to the SMA, as well as several
297 chemical plants. For this reason, easterly wind patterns change the characteristics of the
298 KMA/AMY site from a classical rural site to those resembling an industrial site.

299 At the HUFS/Yongin site, high tropospheric NO_2 VCD values were found under northwesterly
300 wind conditions with wind speeds of 2–6 m/s, as shown in Figure 6c. The HUFS/Yongin site is
301 located on the southeast side of Seoul, making it downwind of Seoul during westerly wind
302 conditions. Under these conditions, the air quality of the surrounding area is dominated by
303 emissions from Seoul. Figure 6c indicates that transport of pollutants from Seoul affected
304 tropospheric NO_2 measurements at the HUFS/Yongin site during the MAPS-Seoul campaign. To
305 further assess transport from Seoul to the HUFS/Yongin site, Figure 7 shows a time series of
306 tropospheric NO_2 VCD along with wind field data at the HUFS/Yongin site during the MAPS-
307 Seoul campaign. Enhanced tropospheric NO_2 VCDs and high wind speed were highly connected
308 under westerly wind conditions. Otherwise, low tropospheric NO_2 values were observed under
309 conditions of weak wind speed or southwesterly winds. Considering the direction of Seoul from
310 the HUFS/Yongin site (Figure 2c), those wind directions causing high tropospheric NO_2 VCD at
311 HUFS/Yongin (~ 285°–345°) indicate that the HUFS/Yongin site was highly affected by NO_2
312 transport from Seoul.

313 Figure 8 shows the correlation of tropospheric NO_2 VCDs between the HUFS/Yongin and
314 Yonsei/SEO sites with consideration of the time difference. Because the distance between the
315 Yonsei/SEO and HUFS/Yongin sites is about 40 km, the transport of NO_2 from Yonsei/SEO to
316 HUFS/Yongin can be assessed using a time lag analysis between data from the two observation
317 sites. For this assessment, tropospheric NO_2 VCD data were selected only for northwesterly wind
318 conditions (a wind direction of 270°–360°) at HUFS/Yongin, based on the relative location of the
319 HUFS/Yongin site from the Yonsei/SEO site. A 3-hour time lag was used on the hourly
320 HUFS/Yongin data for the lag correlation analysis shown in Figure 8. In Figure 8a, no correlation
321 was observed before adjusting for the time lag. Therefore, the tropospheric NO_2 VCDs observed
322 at the same time at the two sites were not significantly related. After adjusting for the 3-hour time
323 lag, however, a significant positive correlation was found with a correlation coefficient (r) of 0.44
324 (Figure 8b). The time lag analysis indicated that tropospheric NO_2 in Seoul affects that at the
325 HUFS/Yongin site within a few hours. As shown in Figure 6c, high tropospheric NO_2 VCDs at
326 the HUFS/Yongin site were found when the wind was northwesterly at 2–6 m/s. Based on the
327 distance between the two observation sites (~40 km) and the wind speed when tropospheric NO_2
328 concentrations were high at the HUFS/Yongin site, an air mass in Seoul would take 2–5 hours to
329 flow to the HUFS/Yongin site.

Figure 9 shows the average and standard deviation of hourly tropospheric NO_2 VCD during the MAPS-Seoul campaign. Because the Pandora instrument uses solar radiation, the temporal observation range is from 7:00 to 18:00, local time. In Figure 9a, a diurnal pattern of tropospheric NO_2 VCDs is clearly seen for Yonsei/SEO. At Yonsei/SEO, NO_2 concentrations were high from 9:00 to 14:00. After high concentrations during the day, NO_2 VCD decreased in the late afternoon. At the HUFS/Yongin site, however, the diurnal pattern of tropospheric NO_2 VCD was different from that in Yonsei/SEO. The tropospheric NO_2 VCD in the afternoon was higher than in the morning. Because of the lower transportation density around the HUFS/Yongin site, no effects on NO_2 VCD due to transportation during the morning rush hour were observed. The significant increase in NO_2 VCD during the afternoon may have been caused by NO_2 advection from Seoul, because the temporal change in tropospheric NO_2 VCD at HUFS/Yongin was highest between 12:00 and 13:00, 3 hours after VCD peaked in Yonsei/SEO. At PNU/Busan, NO_2 was high around noon, but was small compared with that observed at Yonsei/SEO, despite being a populous region. For the three regions in Figure 9a, the diurnal variations in tropospheric NO_2 VCD can be readily explained. However, an explanation of the diurnal variations in the remaining three regions (Figure 9b) is more challenging because these three sites are strongly affected by wind field changes related to emission sources in the vicinity (KMA/AMY and GIST/Gwangju) and trans-boundary transport (NIER/BYI). At NIER/BYI, GIST/Gwangju, and

KMA/AMY, we detected small diurnal variability in tropospheric NO_2 VCD during the MAPS-Seoul campaign.

SUMMARY

NO_2 VCDs were observed at six Pandora observation sites on the Korean Peninsula during the MAPS-Seoul campaign from May to June 2015. To analyze NO_2 concentrations in the troposphere, we estimated the tropospheric NO_2 VCD at the six Pandora sites by subtracting OMI stratospheric NO_2 VCD from Pandora total NO_2 VCD. During the MAPS-Seoul campaign period, large differences in tropospheric NO_2 VCD were found between urban and rural sites. Two urban sites, Yonsei/SEO and PNU/Busan, had large maximum tropospheric NO_2 VCD values of 4.70 DU and 2.04 DU, respectively. However, tropospheric NO_2 VCD at the NIER/BYI site was always below 0.45 DU because of its large distance from emission sources. At the sites within the SMA (Yonsei/SEO and HUFS/Yongin), mean values of tropospheric NO_2 VCD were significantly larger than those at the other sites except for PNU/Busan. This indicates that regional emissions near Seoul significantly contribute to high NO_2 concentrations in the SMA. The tropospheric NO_2 VCD at GIST/Gwangju was comparable to that at KMA/AMY, even though the GIST/Gwangju site is located near an urban area.

To understand major contributors to tropospheric NO_2 VCD at each of the observation sites, the wind field (wind speed and direction) from reanalysis data at each site was analyzed in

368 comparison with the change in NO_2 VCD. Using this method, high tropospheric NO_2 VCDs at
369 each site were found to be related with specific wind speeds and directions. At Yonsei/SEO and
370 PNU/Busan, high tropospheric NO_2 VCD values were directly attributed to large local emissions.
371 At the rural sites, the increase of NO_2 VCDs result primarily from trans-boundary transport
372 (NIER/BYI) or transport from domestic emissions near the observation site (KMA/AMY).
373 Because the location of HUFS/Yongin site is usually downwind of Seoul, high tropospheric NO_2
374 VCDs were found under conditions in which the wind blows directly from Seoul (i.e., strong
375 northwesterly wind). In addition, tropospheric NO_2 VCD between the HUFS/Yongin and
376 Yonsei/SEO sites was significantly correlated when a 3-hour time lag was included. This time lag
377 is similar to the estimated transport time between the two sites, based on the distance between the
378 two sites and the wind speed at which high tropospheric NO_2 VCD occurred. Therefore, it seems
379 clear that the high tropospheric NO_2 VCD at HUFS/Yongin site can be directly attributed to
380 emissions in Seoul.

381 Diurnal patterns in tropospheric NO_2 VCD are evident in Yonsei/SEO and HUFS/Yongin from
382 daytime Pandora measurements, but no significant patterns were observed for NIER/BYI,
383 KMA/AMY, and GIST/Gwangju. Although the Yonsei/SEO and HUFS/Yongin sites show
384 diurnal variations in tropospheric NO_2 VCD, the nature of the variations differs between the two
385 sites. At Yonsei/SEO, high NO_2 VCDs were found from 9:00 to 14:00. The HUFS/Yongin site

386 did not show peaks in the morning, but high NO_2 VCDs were observed throughout the afternoon
387 because of NO_2 transport from Seoul.

388 Tropospheric NO_2 VCD was analyzed at each site using Pandora observations. Throughout the
389 campaign period, the SMA had higher NO_2 VCD than other areas in general. The lowest NO_2
390 value was observed at NIER/BYI. The relationship between NO_2 VCD and wind field was
391 analyzed to investigate the effects of regional emissions and transport on the observation sites.
392 The HUFS/Yongin site was significantly affected by the transport of emissions from Seoul.
393 Although several notable results were obtained during this work, the analysis was limited to the
394 period of the MAPS-Seoul campaign. Therefore, further analyses of variations in tropospheric
395 NO_2 using data that span several years are required in the future.

396

397 **ACKNOWLEDGMENTS**
398

399 This subject is supported by Korea Ministry of Environment (MOE) as "Public Technology
400 Program based on Environmental Policy (2017000160001)". We thank the site managers for
401 installing and operating Pandora spectrometers in Korea during the MAPS-Seoul campaign
402 period.

403

404 **REFERENCES**
405

406 Allen, D., Pickering, K., Duncan, B., Damon, M. (2010). Impact of lightning NO emissions on
407 North American photochemistry as determined using the Global Modeling Initiative (GMI)
408 model, *J. Geophys. Res.*, 115: D22301, doi:10.1029/2010JD014062.
409 Baek, K., Kim, J. H., Herman, J. R., Haffner, D. P., and Kim, J. (2017). Validation of Brewer and
410 Pandora measurements using OMI total ozone, *Atmos. Env.*, 160: 165-175.
411 Barthe, C., Pinty, J. –P., and Mari, C. (2007). Lightning-produced NO_x in an explicit electrical
412 scheme tested in a Stratosphere-Troposphere Experiment: Radiation, Aerosols, and Ozone case
413 study, *J. Geophys. Res.*, 112: D04302, doi:10.1029/2006JD007402.
414 Barton, P. K., and Atwater, J. W. (2002). Nitrous Oxide Emissions and the Anthropogenic
415 Nitrogen in Wastewater and Solid Waste, *J. Environ. Eng.*, 128(2): 137-150.
416 Bayram, H., Sapsford, R. J., Abdelaziz, M. M., and Khair, O. A. (2001). Effect of ozone and
417 nitrogen dioxide on the release of proinflammatory mediators from bronchial epithelial cells of
418 nonatopic nonasthmatic subjects and atopic asthmatic patients in vitro, *J. Allergy Clin.*
419 *Immunol.*, 107(2): 287-294.
420 Boersma, K. F., Eskes, H. J., and Brinksma, E. J. (2004). Error analysis for tropospheric NO_2
421 retrieval from space, *J. Geophys. Res.*, 109: D04311, doi:10.1029/2003JD003962.

422 Brasseur, G. P., Hauglustaine, D. A., Walters, S., Rasch, P. J., Muller, J. F., Granier, C., and Tie,
423 X. X. (1998). MOZART, a global chemical transport model for ozone and related chemical
424 tracers 1: Model description, *J. Geophys. Res.*, 103(D21): 28,265–28,289.
425 Brewer, A. W., McElroy, C. T., and Kerr, J. B. (1973). Nitrogen dioxide concentrations in the
426 atmosphere, *Nature*, 246(5429): 129–133.
427 Buchard, V., Brogniez, C., Auriol, F., Bonnel, B., Lenoble, J., Tanskanen, A., Bojkov, B., and
428 Veefkind, P. (2008). Comparison of OMI ozone and UV irradiance data with ground-based
429 measurements at two French sites, *Atmos. Chem. Phys.*, 8: 4517-4528.
430 Bucsela, E. J., Krotkov, N. A., Celarier, E. A., Lamsal, L. N., Swartz, W. H., Bhartia, P. K.,
431 Boersma, K. F., Veefkind, J. P., Gleason, J. F., and Pickering, K. E. (2013). A new
432 stratospheric and tropospheric NO_2 retrieval algorithm for nadir-viewing satellite instruments:
433 applications to OMI, *Atmos. Meas. Tech.*, 6: 2607–2626, doi:10.5194/amt-6-2607-2013.
434 Castellanos, P., Boersma, K. F., Torres, O., and de haan, J. F. (2015). OMI tropospheric NO_2 air
435 mass factors over South America: effects of biomass burning aerosols, *Atmos. Meas. Tech.*, 8:
436 3831-3849.
437 Cede, A. (2011). *Manual for Pandora Software Suite Version 1.3*.

438 Cede, A., Herman, J., Richter, A., Krotkov, N., and Burrows, J. (2006). Measurements of
439 nitrogen dioxide total column amounts using a Brewer double spectrophotometer in direct sun
440 mode, *J. Geophys. Res.*, 111: D05304, doi:10.1029/2005JD006585.
441 Chimot, J., Vlemmix, T., Veefkind, J. P., de Haan, J. F., and Levelt, P. F. (2016). Impact of
442 aerosols on the OMI tropospheric NO_2 retrievals over industrialized regions: how accurate is
443 the aerosol correction of cloud-free scenes via a simple cloud model?, *Atmos. Meas. Tech.*, 9,
444 359-382.
445 Chitano, P., Hosselet, J., Mapp, C., and Fabbri, L. (1995). Effect of oxidant air pollutants on the
446 respiratory system: insights from experimental animal research, *European respiratory journal*,
447 8(8): 1357-1371.
448 Choi, Y., Wang, Y., Zeng, T., Cunnold, D., Yang, E.-S., Martin, R., Chance, K., Thouret, V., and
449 Edgerton, E. (2008). Springtime transitions of NO_2, CO, and O_3 over North America: Model
450 evaluation and analysis, *J. Geophys. Res.*, 113: D20311, doi:10.1029/2007JD009632.
451 Choi, Y., Kim, J., Eldering, A., Osterman, G., Yung, Y. L., Gu, Y., and Liou, K. N. (2009).
452 Lightning and anthropogenic NO_x sources over the United States and the western North
453 Atlantic Ocean: Impact on OLR and radiative effects, *Geophys. Res. Lett.*, 36: L17806,
454 doi:10.1029/2009GL039381.

455 Crutzen, P. J. (1979). The role of No and NO_2 in the chemistry of the troposphere and
456 stratosphere, Ann. Rev., *Earth Planet. Sci.*, 7: 443-472.
457 Dee, D. P., Uppala, S. M., Simmons, A. J., Berrisford, P., Poli, P., Kobayashi, S., Andrae, U.,
458 Balmaseda, M. A., Balsamo, G., Bauer, P., Bechtold, P., Beljaars, A. C. M., van de Berg, L.,
459 Bidlot, J., Bormann, N., Delsol, C., Dragani, R., Fuentes, M., Geer, A. J., Haimberger, L.,
460 Healy, S. B., Hersbach, H., Hólm, E. V., Isaksen, L., Kållberg, P., Köhler, M., Matricardi, M.,
461 McNally, A. P., Monge-Sanz, B. M., Morcrette, J.-J., Park, B.-K., Peubey, C., de Rosnay, P.,
462 Tavolato, C., Thépaut, J.-N. and Vitart, F. (2011). The ERA-Interim reanalysis: configuration
463 and performance of the data assimilation system. *Q.J.R. Meteorol. Soc.*, 137: 553–597.
464 doi:10.1002/qj.828
465 Diemoz, H., Siani, A. M., Redonas, A., Savastiouk, V., McElroy, C. T., Navarro-Comas, M., and
466 Hase, F. (2014). Improved retrieval of nitrogen dioxide (NO_2) column densities by means of
467 MKIV Brewer spectrophotometers, *Atmos. Meas. Tech.*, 7: 4009-4022.
468 Donnelly, A. A., Broderick, B. M., and Misstear. B. D. (2015). The effect of long-range air mass
469 transport pathways on PM10 and NO_2 concentrations at urban and rural background sites in
470 Ireland: Quantification using clustering techniques, J. Environ. Sci. and Health, Part A, 50(7):
471 647-658.

472 Galloway, J. N., Dentener, F. J., Capone, D. G., Boyer, E. W., Howarth, R. W., Seitzinger, S. P.,
473 Asner, G. P., Cleveland, C. C., Green, P. A., Holland, E. A., Karl, D. M., Michaels, A. F.,
474 Porter, J. H., Townsend, A. R., and Voeroesmarty, C. J. (2004). Nitrogen cycles: past, present,
475 and future, Biogeochemistry, 70: 153-226.
476 Herman, J., Cede, A., Spinei, E., Mount, G., Tzortziou, M., and Abuhassan, N. (2009). NO_2
477 column amounts from ground-based Pandora and MFDOAS spectrometers using the direct-
478 sun DOAS technique: Intercomparisons and application to OMI validation, *J. Geophys. Res.*,
479 114(D13): D13307, doi:10.1029/2009JD011848.
480 Hudman, R. C., Jacob, D. J., Turquety, S., Leibensperger, E. M., Murray, L. T.,Wu, S., Gilliland,
481 A. B., Avery, M., Bertram, T. H., Brune, W., Cohen, R. C., Dibb, J. E., Flocke, F. M., Fried, A.,
482 Holloway, J., Neuman, J. A., Orville, R., Perring, A., Ren, X., Sachse, G.W., Singh, H. B.,
483 Swanson, A., and Wooldridge, P. J. (2007). Surface and lightning sources of nitrogen oxides
484 over the United States: magnitudes, chemical evolution, and outflow, *J. Geophys. Res.*, 112:
485 D12S05, doi:10.1029/2006JD007912.
486 Ialongo, I., Herman, J., Krotkov, N., Lamsal, L., Boersma, K. F., Hovila, J., and Tamminen, J.
487 (2016). Comparison of OMI NO_2 observations and their seasonal and weekly cycles with
488 ground-based measurements in Helsinki. *Atmos. Meas. Tech.*, 9(10): 5203-5212.

489 Intergovernmental Panel on Climate Change (IPCC) (2007). *Contribution of Working Group I to*
490 *the Fourth Assessment Report of the Intergovernmental Panel on Climate Change, in Climate*
491 *Change 2007: The Physical Science Basis,* edited by S. Solomon et al., 996 pp., Cambridge
492 Univ. Press, Cambridge, U. K.
493 Irie, H., Kanaya, Y., Akimoto, H., Tanimoto, H., Wang, Z., Gleason, J. F., and Bucsela, E. J.
494 (2008). Validation of OMI tropospheric NO_2 column data using MAX-DOAS measurements
495 deep inside the North China Plain in June 2006: Mount Tai Experiment 2006, *Atmos. Chem.*
496 *Phys.*, 8: 6577-6586, https://doi.org/10.5194/acp-8-6577-2008.
497 Kerr, J. B. (1989). *Ground-based measurements of nitrogen dioxide using the Brewer*
498 *spectrophotometer*, in: Ozone in the Atmosphere, Vol. 1, 340 pp.
499 Kerr, J. B., Asbridge, I. A., and Evans, W. F. J. (1988). Intercomparison of total ozone measured
500 by the Brewer and Dobson spectrophotometers at Toronto, *J. Geophys. Res.*, 93: 11129-11140.
501 Kim, J. (2012). GEMS (Geostationary Environmental Monitoring Spectrometer) onboard the
502 GeoKOMPSAT to monitor air quality in high temporal and spatial resolution over Asia-Pacific
503 Region, in: EGU General Assembly Conference Abstracts, Vol. 14, 4051 pp.
504 Kim, J., Kim, J., Cho, H. –K., Herman, J., Park, S. S., Lim, H. K., Kim, J. –H., Miyagawa, K.,
505 and Lee, Y. G. (2017). Intercomparison of total column ozone data from the Pandora

506 Spectrophotometer with Dobson, Brewer and OMI measurements over Seoul, Korea, *Atmos.*
507 *Meas. Tech.*, 10, 3661-3676, https://doi.org/10.5194/amt-10-3661-2017.
508 Knepp. T., Pippin, M., Crawford, J., Chen, G., Szykman, J., Long, R., Cowen, L., Cede, A.,
509 Abuhassan, N., Herman, J., Delgado, R., Compton, J., Berkoff, T., Fishman, J., Martins, D.,
510 Stauffer, R., Thompson, A., Weinheimer, A., Knapp, D., Montzka, D., Lenschow, D., Neil, D.
511 (2015). Estimating surface NO_2 and SO_2 mixing ratios from fast-response total column
512 observations and potential application to geostationary missions, *J. Atmos. Chem.*, 72:261-286.
513 Kollonige, D. E., Thompson, A. M., Josipovic, M., Tzortziou, M., Beukes, J. P., Burger,
514 R., Martins, D. K., van Zyl, P. G., Vakkari, V. & Laakso, L. (2017*). OMI satellite and ground-*
515 *based Pandora observations and their application to surface NO2 estimations at terrestrial*
516 *and marine sites. Journal of Geophysical Research: Atmospheres*, 122, doi:
517 10.1002/2017JD026518.
518 Krotkov, N. A., Lamsal, L. N., Celarier, E. A., Swartz, W. H., Marchenko, S. V., Bucsela, E. J.,
519 Chan, K. L., Wenig, M., and Zara, M. (2017). The version 3 OMI NO_2 standard product,
520 *Atmos. Meas. Tech.*, 10:3133-3149.
521 Lee, D. S., Koehler, J., Grobler, E., Rohrer, F., Sausen, R., Gallardo-Klenner, L., Olivier, J. G. J.,
522 Dentener, F. J., and Bouwman, A. F. (1997). Estimations of global NOx emissions and their
523 uncertainties, *Atmos. Env.*, 31(12): 1735-1749.

524 Lee, H., Irie, H., Kim, Y. J., Noh, Y., Lee, C., Kim, Y., and Chun, K. J. (2009a). Retrieval of
525 aerosol extinction in the lower troposphere based on UV MAX-DOAS measurements, *Aerosol*
526 *Sci. Technol.*, 43(5): 502-509.
527 Lee, H., Kim, Y. J., Jung, J., Lee, C., Heue, K.-P., Platt, U., Hu, M., and Zhu, T. (2009b). Spatial
528 and temporal variations in NO_2 distributions over Beijing, China measured by imaing
529 differential optical absorption spectroscopy, *J. Env., Manage.*, 90(5): 1814-1823.
530 Lee, H. –J., Kim, S. –W., Brioude, J., Cooper, O. R., Frost, G. J., Kim, C. –H., Park, R. J.,
531 Trainer, M., and Woo, J. –H. (2014), Transport of NOx in East Asia identified by satellite and
532 in situ measurements and Lagrangian particle dispersion model simulations, *J. Geophys. Res.*,
533 doi:10.1002/2013JD021185.
534 Levelt, P. F., Van den Oord, G. H., Dobber, M. R., Malkki, A., Visser, H., De Vries, J., Stammes,
535 P., Lundell, J. O., and Saari, H. (2006). The ozone monitoring instrument, *IEEE Trans. Geosci.*
536 *and rem. Sens.*, 44: 1093-1101.
537 Liley, J. B., Johnston, P. V., McKenzie, R. L., Thomas, A. J., and Boyd, I. S. (2000).
538 Stratospheric NO2 variations from a long time series at Lauder, New Zealand, J. *Geophys. Res.*,
539 105(D9): 11,633 – 11,640.
540 Noxon, J. F. (1979). Stratospheric NO_2 global behavior, *J. Geophys. Res.*, 84(C8): 5067–5076.
541 Seinfeld, J. H. (1988). Ozone air quality models, *JAPCA*, 38(5): 616-645.

542 Seinfeld, J. H., and Pandis, S. N. (2012). *Atmospheric chemistry and physics: from air pollution*
543 *to climate change*, John Wiley & Sons, 225 pp.
544 Sinreich, R., Friess, U., Wagner, T., and Platt, U. (2005). Multi axis differential optical
545 absorption spectroscopy (MAX-DOAS) of gas and aerosol distributions, *Faraday Discuss*, 130:
546 153-164.
547 Solomon, S., Portmann, R. W., Sanders, R. W., Daniel, J. S., Madsen, W., Bartram, B., and
548 Dutton, E. G. (1999). On the role of nitrogen dioxide in the absorption of solar radiation, *J.*
549 *Geophys. Res.*, 104(D10): 12047-12058.
550 Tzortziou, M., Herman, J. R., Cede, A. and Abuhassan, N. (2012). High precision, absolute total
551 column ozone measurements from the Pandora spectrometer system: Comparisons with data
552 from a Brewer double monochromator and Aura OMI, *J. Geophys. Res.*, 117(D16): D16303,
553 doi:10.1029/2012JD017814.
554 Tzortziou, M., Herman, J. R., Cede, A., Loughner, C. P., Abuhassan, N., and Naik, S. (2013).
555 Spatial and temporal variability of ozone and nitrogen dioxide over a major urban estuarine
556 ecosystem, *J. Atmos. Chem.*, 72: 287-309.
557 Van Roozendael, M., de Maziere, M., Hermans, C., Simon, P. C., Pommereau, J. P., Goutail, F.,
558 Tie, X. X., Brasseur, G. and Granier, C. (1997). Ground-based observations of stratospheric

559 NO_2 at high and midlatitudes in Europe after the Mount Pinatubo eruption, *J. Geophys. Res.*,
560 102 (D15): 19,171 – 19,176.
561 von Klot, S., Peters, A., Aalto, P., Bellander, T., Berglind, N., D'Ippoliti, D., Elosua, R.,
562 Hörmann, A., Kulmala, M., and Lanki, T. (2005). Ambient air pollution is associated with
563 increased risk of hospital cardiac readmissions of myocardial infarction survivors in five
564 European cities, *Circulation*, 112(20): 3073-3079.
565 Wenig, M., Kuhl, S., Beirle, S., Bucsela, E., Jahne, B., Platt, U., Gleason, J., Wagner, T. (2004).
566 Retrieval and analysis of stratospheric NO_2 from the Global Ozone Monitoring Experiment, *J.*
567 *Geophys. Res.*, 109(D4): doi:10.1029/2003JD003652.
568 Yun, S., Lee, H., Kim, J., Jeong, U., Park, S. S., and Herman, J. (2013). Inter-comparison of NO_2
569 column densities measured by Pandora and OMI over Seoul, Korea, *Kor. J. Rem. Sens.*, 29:
570 663-670.
571 Zhang, R., Sanger, N. T., Orville, R. E., Tie, X., Randel, W., Williams, E. R. (2000). Enhanced
572 NO_x by lightning in the upper troposphere and lower stratosphere inferred from the UARS
573 Global NO2 measurements, Geophys. Res. Lett., 27(5): 685-688.
574 Zhang, X., Helsdon, J. H., and Farley, R. D. (2003). Numerical modeling of lightning-produced
575 NO_x using an explicit lightning scheme: 2. Three dimensional simulation and expanded
576 chemistry, J. Geophys. Res., 108(D18): 4580, doi:10.1029/2002JD003225.

577

List of table titles

579 Table 1. Location and altitude of each Pandora site during the MAPS-Seoul campaign.

580 Table 2. The statistics of tropospheric NO_2 VCD at each Pandora site during the MAPS-Seoul
581 campaign. (Unit: DU).

582

List of figure captions

584 Figure 1. Locations of the Pandora sites on the Korean Peninsula with a ten-year (2005–2014)
585 mean tropospheric NO_2 VCD from OMI in May and June, and mean surface wind reanalysis data
586 from ECMWF for the same period.

587 Figure 2. Local characteristics of the Pandora sites at (a) NIER/BYI, (b) Yonsei/SEO, (c)
588 HUFS/Yongin, (d) KMA/AMY, (e) GIST/Gwangju, and (f) PNU/Busan. The radius of each red
589 circle is 0.125°, representing the resolution of the wind field we employed, and the center of it
590 indicates the location of each Pandora (red dot). The location of Pandora at Yonsei/SEO is
591 marked in green on (c).

592 Figure 3. (a) Total VCD of NO_2 observed from Pandora and (b) sampled stratospheric NO_2 from
593 OMI at each site during the MAPS-Seoul campaign. Box-and-whisker plots show 10, 25, 50, 75,

and 90 percentiles, and the dots indicate the means. The red box with broken lines in (a) represents the y-axis range of (b).

Figure 4. Tropospheric NO_2 VCDs obtained from Pandora observations at the (a) NIER/BYI, (b) Yonsei/SEO, (c) HUFS/Yongin, (d) KMA/AMY, (e) GIST/Gwnagju, and (f) PNU/Busan sites during the MAPS-Seoul campaign. The red broken line in (a) indicates 0 DU.

Figure 5. Tropospheric NO_2 VCD at each Pandora site. Box-and-whisker plots show 10, 25, 50, 75, and 90 percentiles, and the dots indicate the means.

Figure 6. Polar plots of tropospheric NO_2 VCD for the (a) NIER/BYI, (b) Yonsei/SEO, (c) HUFS/Yongin, (d) KMA/AMY, (e) GIST/Gwangju, and (f) PNU/Busan sites, along with wind conditions during the MAPS-Seoul campaign (Unit: DU).

Figure 7. Time series of tropospheric NO_2 VCD, wind speed, and wind direction at the HUFS/Yongin site.

Figure 8. Scatter plots of tropospheric NO_2 VCDs between the Yonsei/SEO and HUFS/Yongin sites (a) without consideration of time lag, and (b) with a time lag of 3 hours under northwesterly wind conditions at the HUFS/Yongin site.

Figure 9. Diurnal variations in tropospheric NO_2 at (a) Yonsei/SEO, HUFS/Yongin, and PNU/Busan, and (b) GIST/Gwangju, NIER/BYI and KMA/AMY, based on hourly averaged data. The error bars represent the standard deviations; the red broken line in (b) indicates 0 DU.

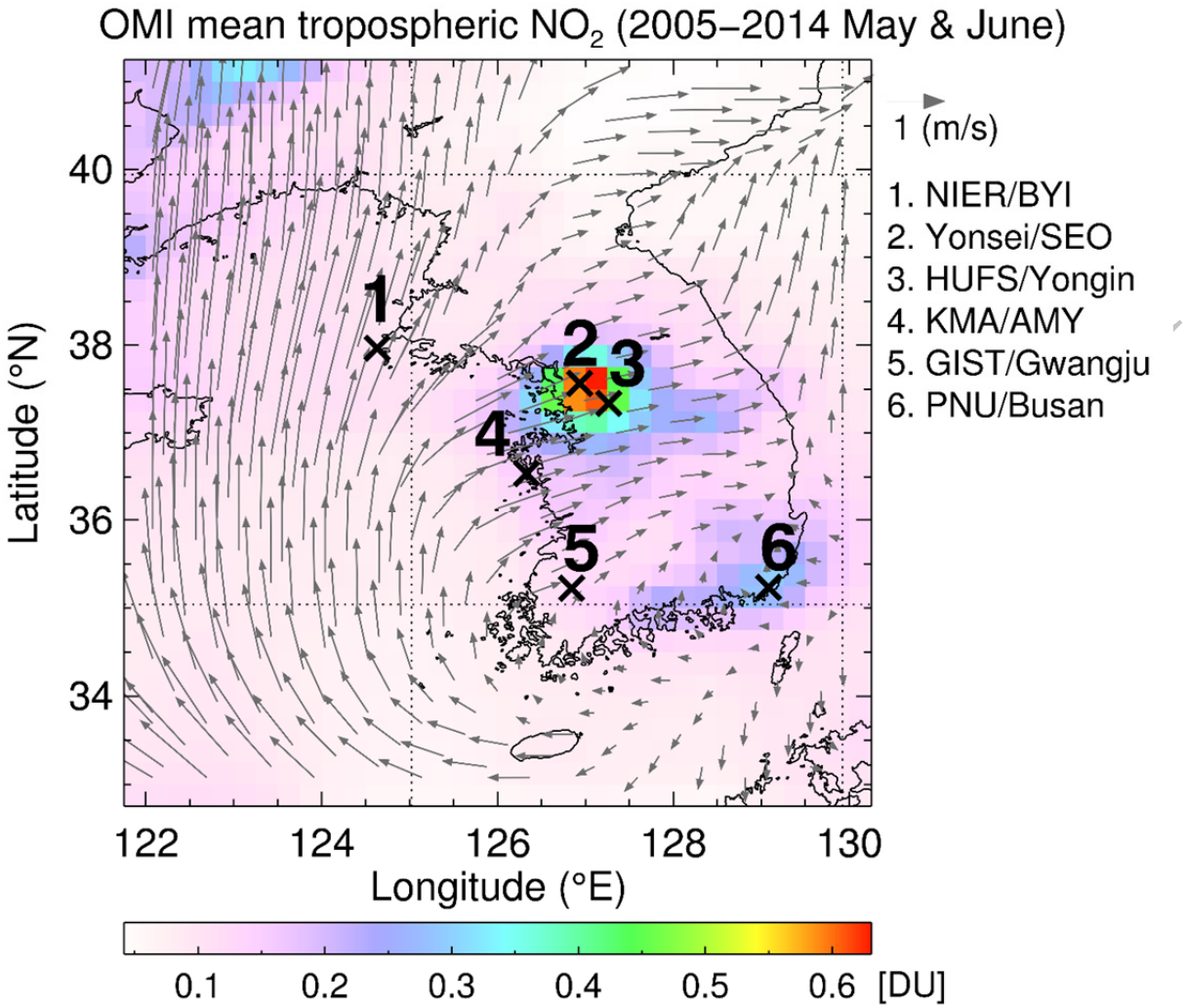

Figure 1. Locations of the Pandora sites on the Korean Peninsula with a ten-year (2005–2014) mean tropospheric NO_2 VCD from OMI in May and June, and mean surface wind reanalysis data from ECMWF for the same period.

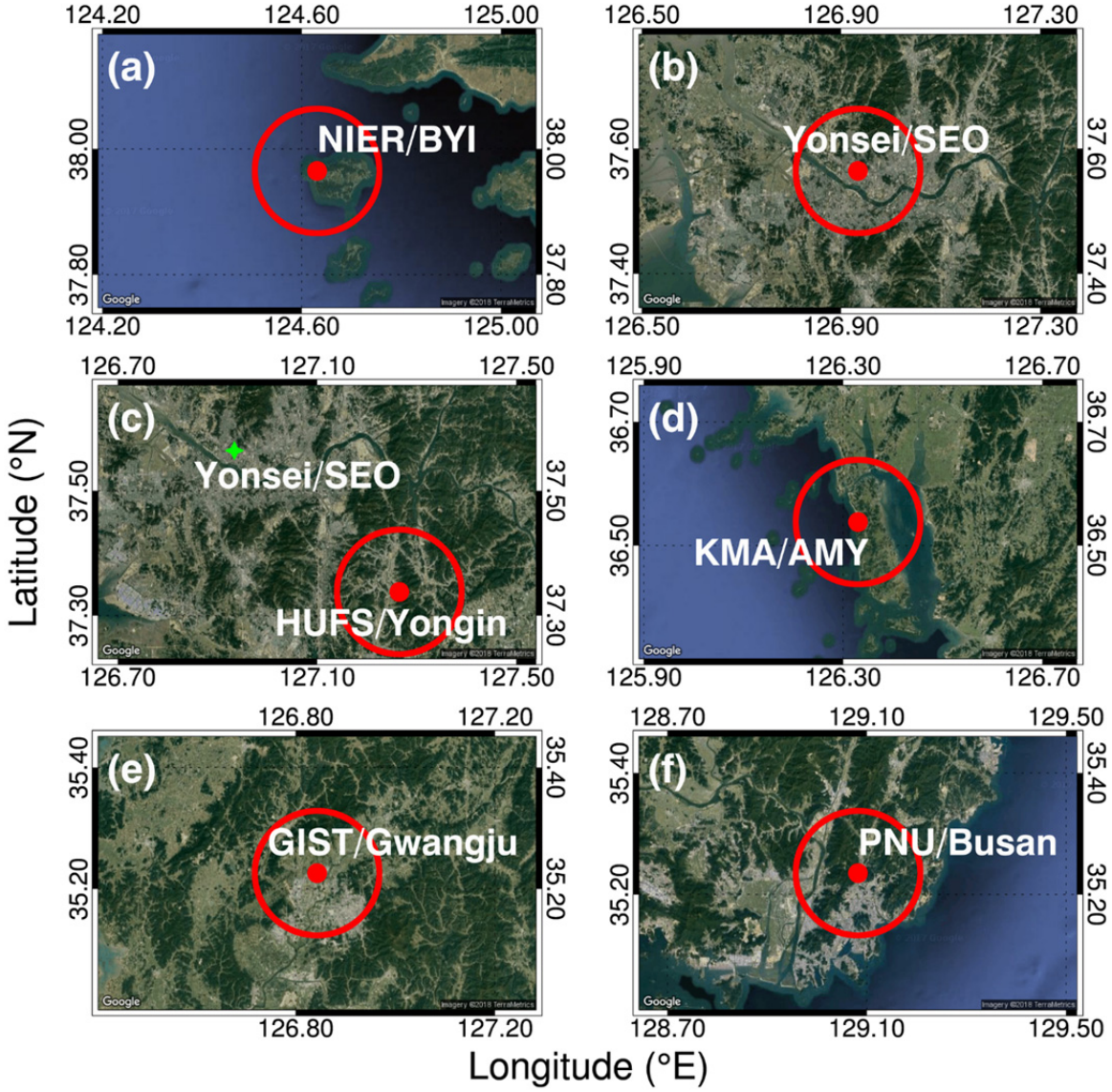

Figure 2. Local characteristics of the Pandora sites at (a) NIER/BYI, (b) Yonsei/SEO, (c) HUFS/Yongin, (d) KMA/AMY, (e) GIST/Gwangju, and (f) PNU/Busan. The radius of each red circle is 0.125°, representing the resolution of the wind field we employed, and the center of it indicates the location of each Pandora (red dot). The location of Pandora at Yonsei/SEO is marked in green on (c).

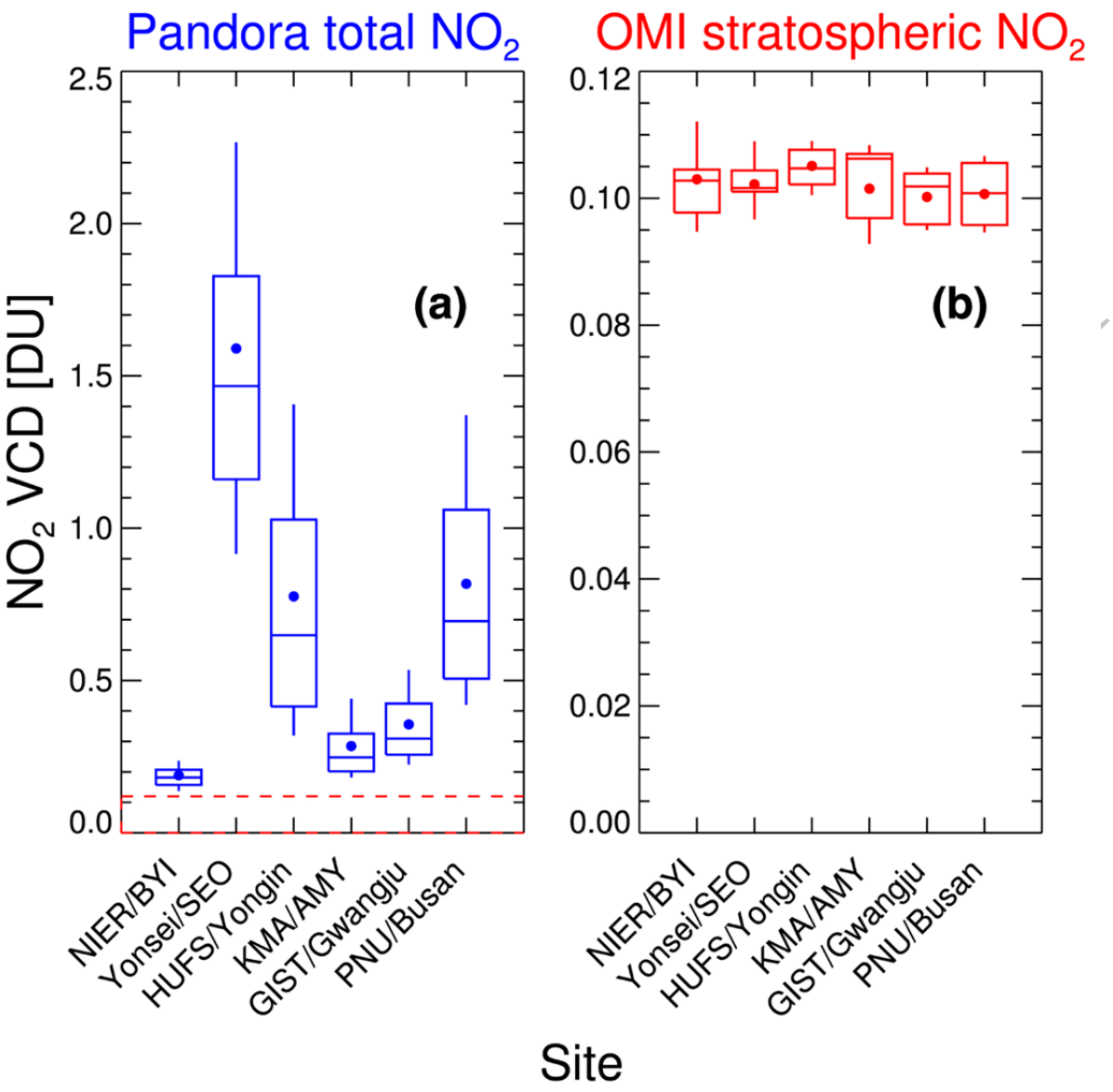

Figure 3. (a) Total VCD of NO_2 observed from Pandora and (b) sampled stratospheric NO_2 from OMI at each site during the MAPS-Seoul campaign. Box-and-whisker plots show 10, 25, 50, 75, and 90 percentiles, and the dots indicate the means. The red box with broken lines in (a) represents the y-axis range of (b).

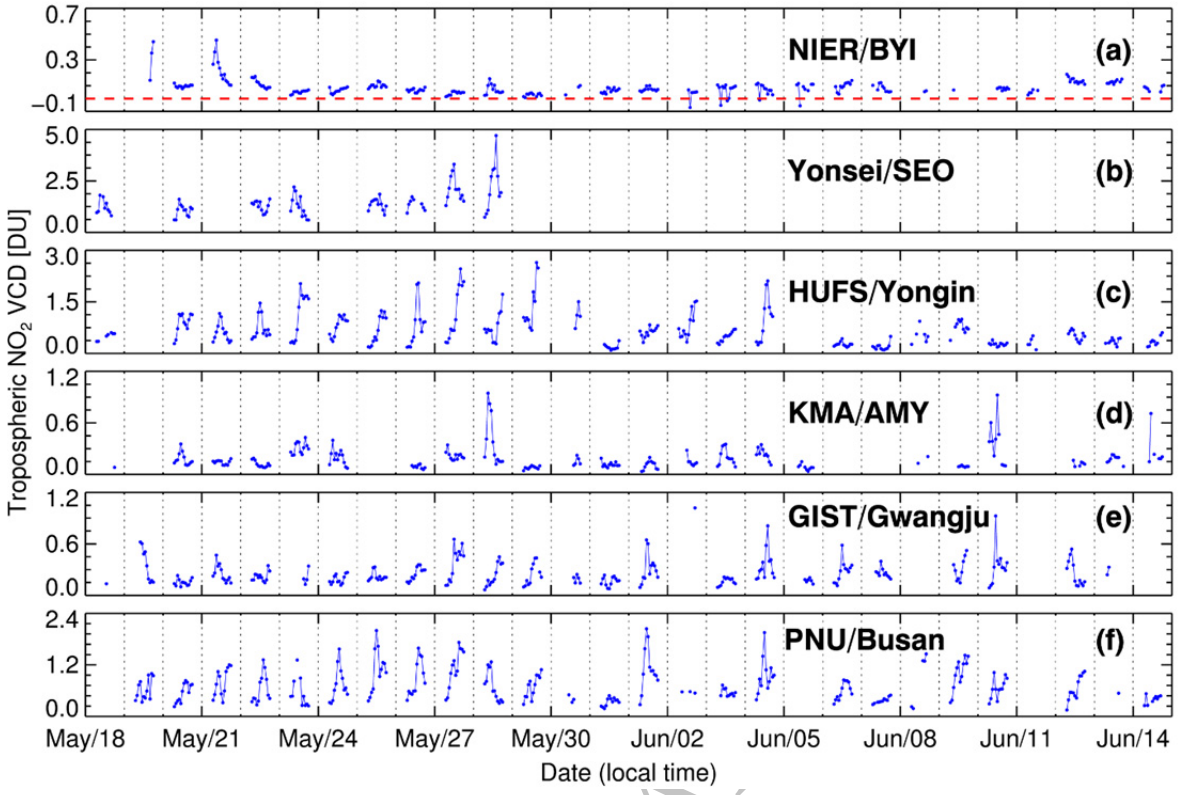

Figure 4. Tropospheric NO_2 VCDs obtained from Pandora observations at the (a) NIER/BYI, (b) Yonsei/SEO, (c) HUFS/Yongin, (d) KMA/AMY, (e) GIST/Gwnagju, and (f) PNU/Busan sites during the MAPS-Seoul campaign. The red broken line in (a) indicates 0 DU.

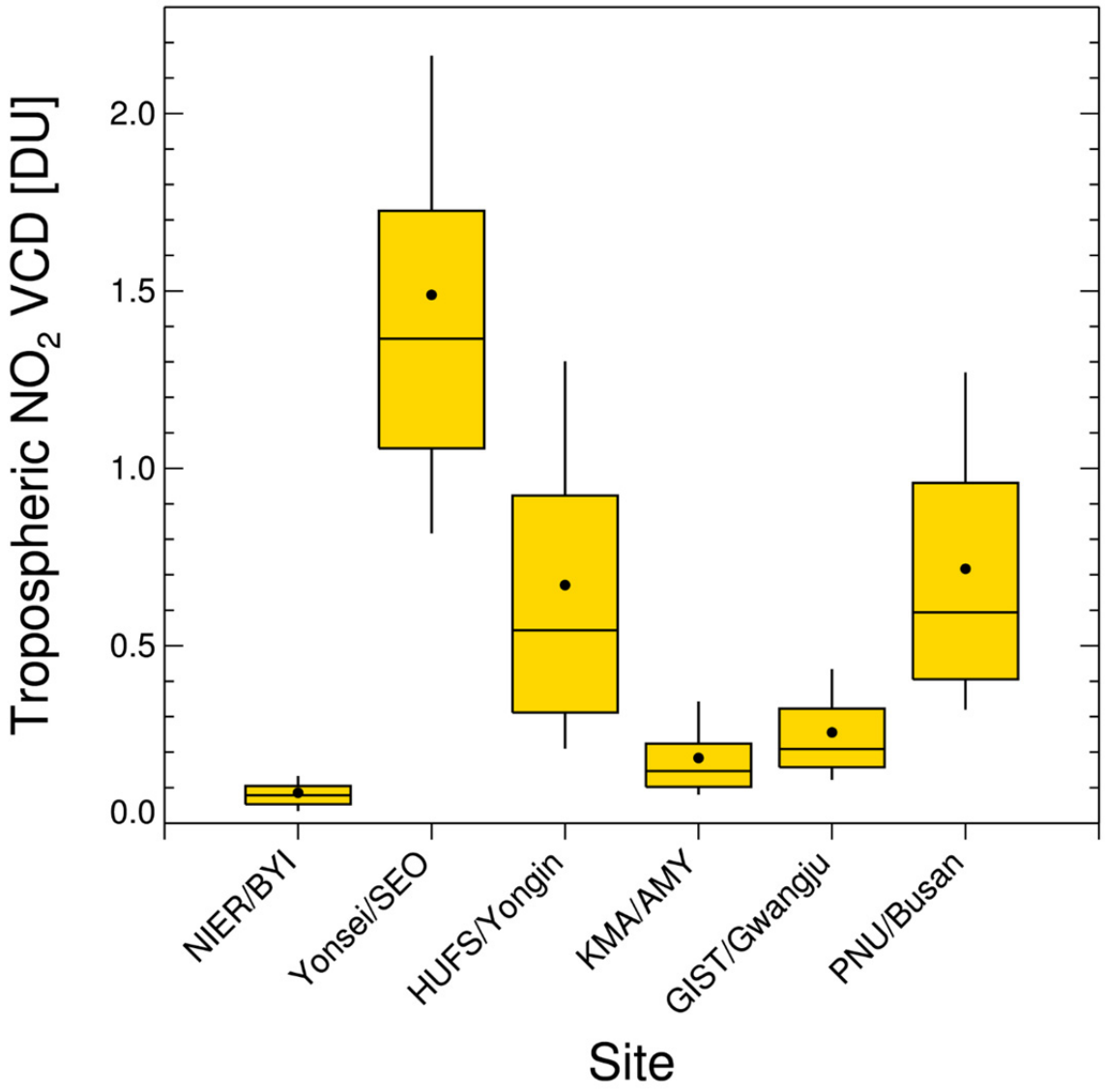

Figure 5. Tropospheric NO_2 VCD at each Pandora site. Box-and-whisker plots show 10, 25, 50, 75, and 90 percentiles, and the dots indicate the means.

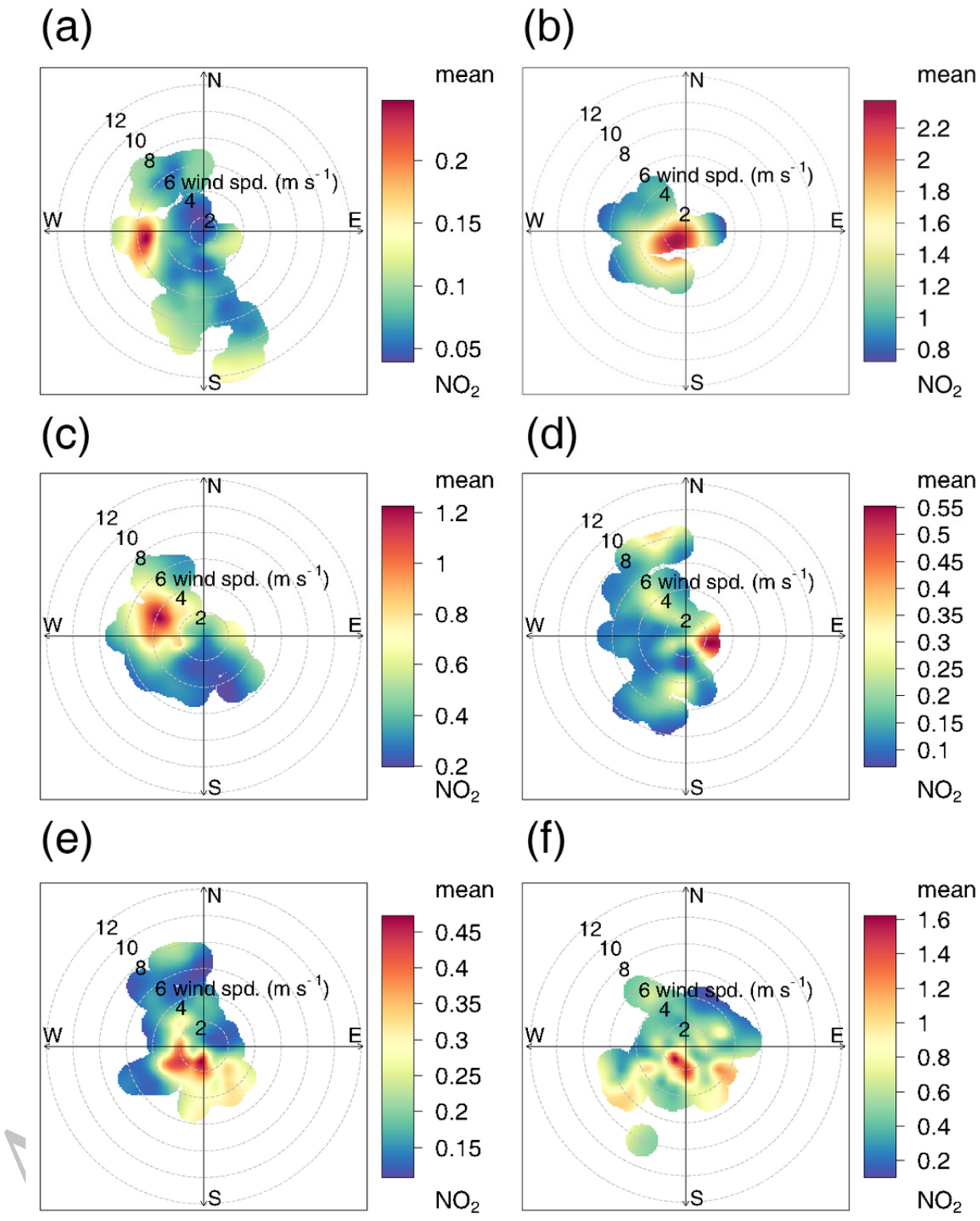

Figure 6. Polar plots of tropospheric NO_2 VCD for the (a) NIER/BYI, (b) Yonsei/SEO, (c) HUFS/Yongin, (d) KMA/AMY, (e) GIST/Gwangju, and (f) PNU/Busan sites, along with wind conditions during the MAPS-Seoul campaign (Unit: DU).

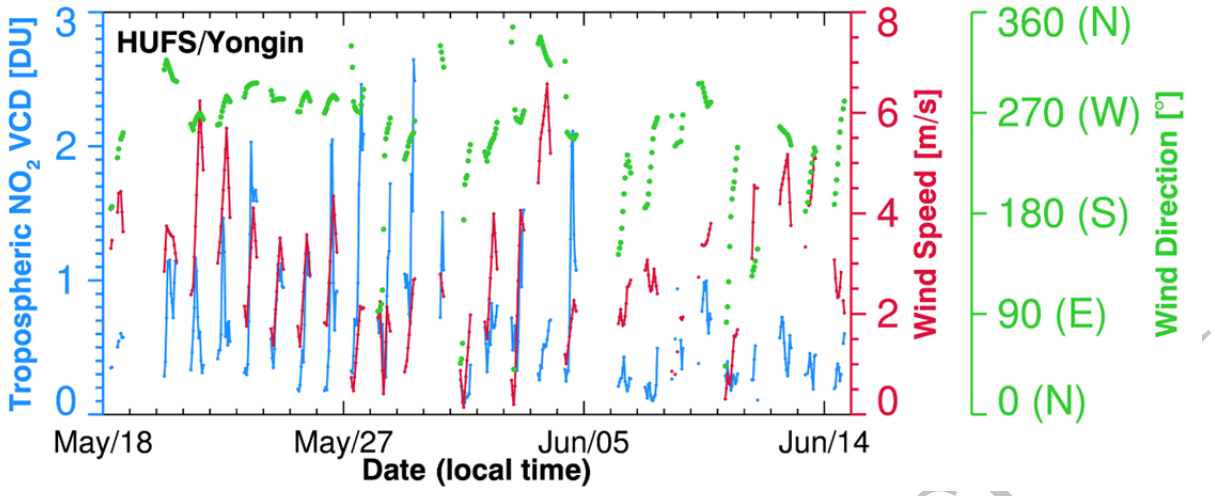

Figure 7. Time series of tropospheric NO_2 VCD, wind speed, and wind direction at the HUFS/Yongin site.

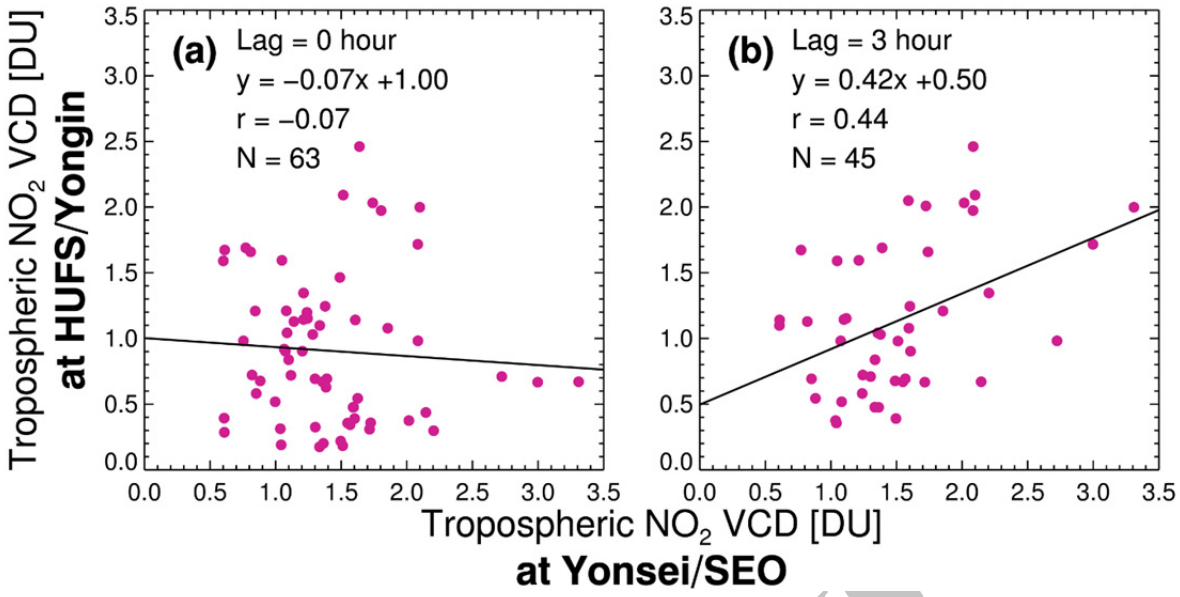

Figure 8. Scatter plots of tropospheric NO_2 VCDs between the Yonsei/SEO and HUFS/Yongin sites (a) without consideration of time lag, and (b) with a time lag of 3 hours under northwesterly wind conditions at the HUFS/Yongin site.

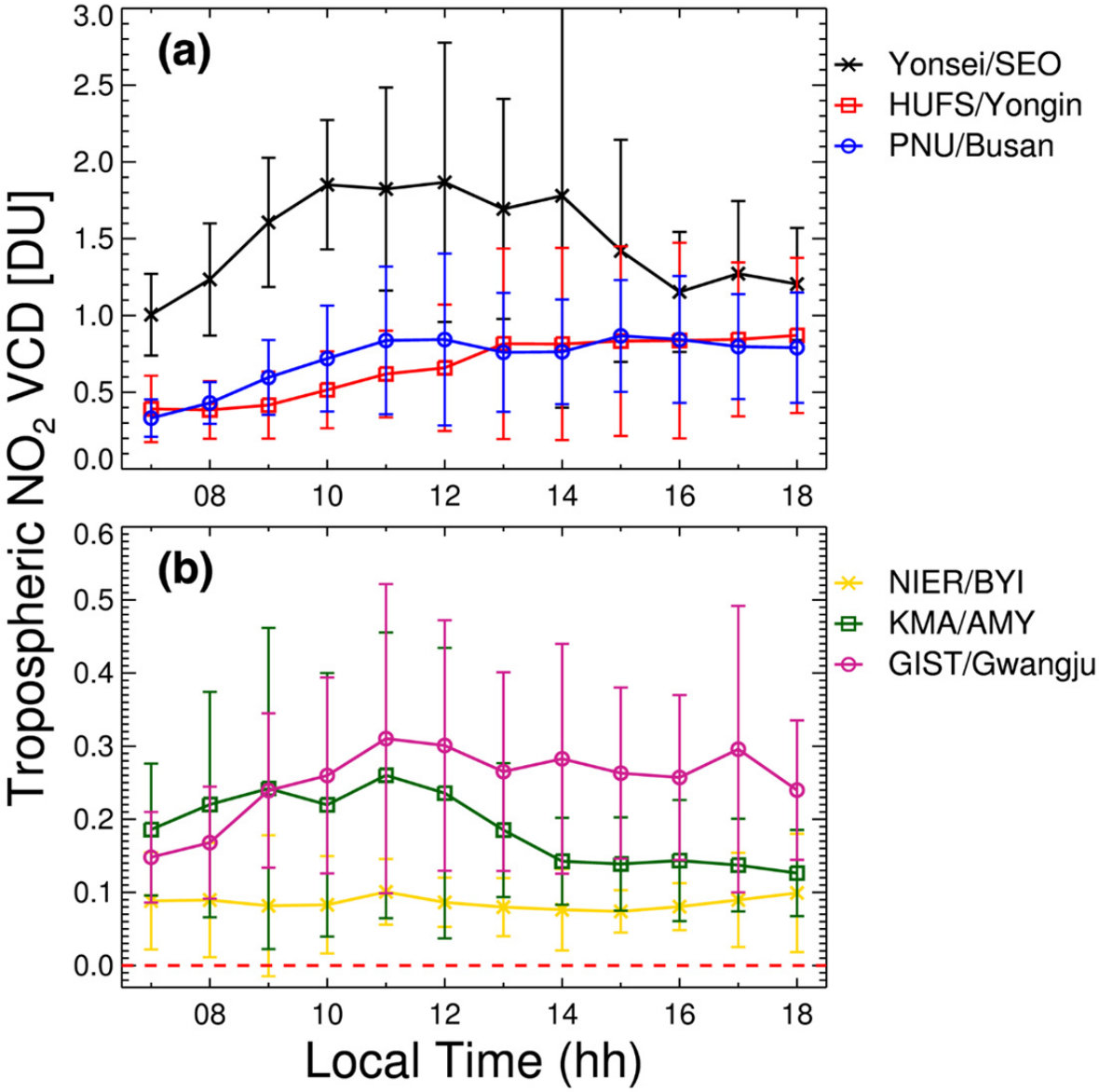

Figure 9. Diurnal variations in tropospheric NO_2 at (a) Yonsei/SEO, HUFS/Yongin, and PNU/Busan, and (b) GIST/Gwangju, NIER/BYI and KMA/AMY, based on hourly averaged data. The error bars represent the standard deviations; the red broken line in (b) indicates 0 DU.

Table 1. Location and altitude of each Pandora site during the MAPS-Seoul campaign.

Site	NIER /BYI	Yonsei /SEO	HUFS /Yongin	KMA /AMY	GIST /Gwangju	PNU /Busan
Longitude (°E)	124.631	126.934	127.265	126.330	126.843	129.083
Latitude (°N)	37.965	37.564	37.338	36.538	35.226	35.235
Altitude (m)	136	88	167	47	52	71

Table 2. The statistics of tropospheric NO_2 VCD at each Pandora site during the MAPS-Seoul campaign. (Unit: DU).

Site	NIER /BYI	Yonsei /SEO	HUFS /Yongin	KMA /AMY	GIST /Gwangju	PNU /Busan
Average	0.09	1.49	0.67	0.18	0.26	0.72
Standard deviation	0.06	0.68	0.49	0.14	0.14	0.39
Maximum (Time)	0.45 (May 21st, 09:00)	4.70 (May 28th, 14:00)	2.65 (May 29th, 15:00)	0.95 (May 28th, 09:00)	1.02 (June 2nd, 17:00	2.04 (June 1st, 11:00)
Minimum (Time)	-0.07 (June 2nd, 14:00)	0.60 (May 20th, 08:00)	0.09 (May 31st, 13:00)	0.03 (June 5st, 15:00)	0.07 (May 28th, 07:00)	0.15 (June 12th, 07:00)
Number of data points	251	88	272	211	238	256